Optimised Online Multi-Sine Battery Electrochemical Impedance Spectroscopy using a Three-Phase Neutral Point Clamped Converter

Kai-Ping Liu
Department of Mechanical Engineering
University of Southampton
Southampton, UK
kpl1e20@soton.ac.uk

Georgios Orfanoudakis
Department of Electrical and Computer Engineering
Hellenic Mediterranean Univ.
Heraklion, Greece
gorfas@hmu.gr

Suleiman M. Sharkh
Department of Mechanical Engineering
University of Southampton
Southampton, UK
s.m.sharkh@soton.ac.uk

Andrew Cruden
Department of Mechanical Engineering
University of Southampton
Southampton, UK
a.j.cruden@soton.ac.uk

***Abstract*—Electrochemical impedance spectroscopy (EIS) is a method that is commonly used for determining the state of charge and state of health of batteries and fuel cells. Historically, it was used offline in research laboratories, but the rapid increase of demand for fuel cells and battery storage to meet the accelerating growth of electric vehicles and renewable energy has stimulated research into online in-situ EIS. This paper presents an online EIS technique integrated within the control and measurement system of a neutral point clamped (NPC) inverter. This is achieved by adding zero-sequence perturbation voltages to the inverter's reference three phase voltages. By connecting the battery midpoint to the neutral point of the inverter, a perturbation current flows into the battery. Measurement of the battery voltage and current and subsequent spectral analysis are used to calculate its impedance. To speed up the EIS measurement, the zero-sequence voltage perturbation includes multiple sinewaves of 5 different frequencies, instead of a single frequency sinewave. Furthermore, the phase angles of the sinewaves are optimised to prevent inverter overmodulation thus preventing distortion of the inverter's output voltage. Detailed simulation results show close alignment of the proposed EIS measurement with theoretical values in the range of 0.01 Hz – 4 kHz, which covers the typical range for batteries and fuel cells' interest frequency on the spectrum.**

Keywords—Electrochemical impedance spectroscopy (EIS), Neutral point clamped (NPC) converter, Zero-sequence.

I. INTRODUCTION

The accelerating growth of electric vehicles and renewable energy sources and the corresponding rapid increase in the demand for batteries has stimulated research in developing rapid online techniques for measuring and monitoring their state of health and state of charge. Electrochemical Impedance Spectroscopy (EIS) is a technique for testing and diagnosing the states of charge and health of batteries and fuel cells [1]. Historically, it was used mainly in research laboratories to investigate the fundamental electromechanical processes, but in recent years it has been deployed in the field. Furthermore, the EIS function is increasingly integrated within the power electronic converters used to interface the batteries to their charging sources or loads, e.g., electric vehicle motors, renewable energy sources and the grid. Most of the relevant EIS studies employ DC/DC converters. In [2], an EIS function is integrated within the control system of a boost converter interfacing a PEM fuel cell to the DC bus. EIS single frequency sweep perturbation is added to the current reference of the converter's controller at high EIS perturbation frequency. In the low EIS frequency range, the signal is added to the voltage control loop reference. Huang et al [3] add the EIS perturbation to the duty cycle of the boost converter. In [4] and [5] EIS functionality is integrated within full-bridge phase shift zero-voltage switching DC/DC converters for PEM fuel cell interface and battery charging, respectively. Islam and Park demonstrated precision EIS implementation in a buck DC/DC battery charger [6]. Wang et al. [7] proposed an EIS system integrated within a dual HB bridge converter for measuring the impedance of series connected lithium batteries. Dam and John [8] discuss the implementation of a high-resolution EIS within a grid connected converter comprising an AC/DC and a DC/DC converter. They proposed using an interleaved DC/DC converter to improve output voltage resolution. In [9] and [10], different interleaved converter topologies and interleaved phase numbers are studied to improve output voltage ripple, as well. Furthermore, Hong et al. [11] proposed a parallel DC/DC converter with one converter used to produce EIS perturbation and the other for controlling the output voltage. This decouples the two functions and mitigates output fluctuations seen for example in [2] – [4], thus enabling continuous operation and removing the need for disconnecting the fuel cell or battery when the EIS function is activated.

When considering practical battery applications, e.g., in high-power electric vehicles, the battery state may change quickly with time and temperature, hence a fast EIS approach may be needed to achieve real-time measurement. The speed of performing the EIS measurement depends on the type of excitation used. Generally, there are two types of signals, as illustrated in Fig. 1: single frequency excitation and broadband excitation. The single-frequency excitation has a strong energy density concentrated in one frequency and a high signal-to-noise ratio (SNR). On the other hand, for broadband excitation, the energy is distributed over a wide range of frequencies on the spectrum of interest, making it more susceptible to background noises than single-frequency excitation. However, the broadband approaches can measure a range of frequencies simultaneously, thus significantly reducing the measurement time.

Table I presents a summary of broadband methods used in converter-based EIS systems reported in recent research papers. Most studies use the multi-sine EIS approach, as thanks to the

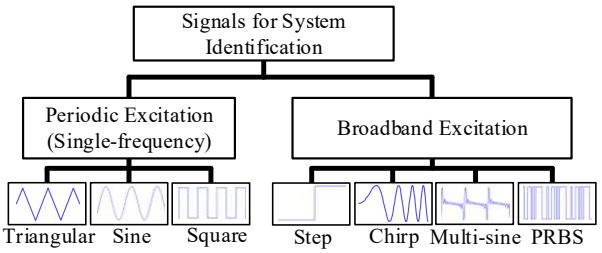

Fig. 1. Types of EIS excitation signals.

orthogonal characteristic of sinusoidal signals, multi-sine excitation can be easily implemented. In [12] – [16], the number of sinewaves range from three to seventeen, while it can be ever higher. However, in-situ converter-based EIS should also consider the impact on the converter's primary function and the quality of its output and losses. The greater the number of sine frequencies included, the higher the total amplitude of the multi-sine injected into the control reference, which can result in output distortion. To address this issue, [12] uses the generalised reduced gradient method to minimise the multi-sine peak containing seventeen frequencies. In addition, [14] mentions that adjustment of the phase shifts of frequencies involved can also minimise the summation amplitude of a multi-sine signal.

Time-variant frequency sine chirp excitation is studied for the converter-based EIS methods in [14], [17]. The short-time Fourier transform (STFT) is used in the signal extraction process to acquire the maximum possible information from the chirp signal. The characteristic of the chirp signal is such that its energy is concentrated at the high frequency end, leading to a poor SNR in the low-frequency spectrum.

Other broadband methods, like step excitation and random binary excitation, are also investigated in [18] – [20]. The step excitation is similar in theory to the multi-sine but with the amplitude decreasing with the order of harmonics. The signal energy density is therefore concentrated on the fundamental and low-order harmonics and has poor SNR at high frequency. The spectrum's signal energy density distribution and signal amplitude affect the EIS performance. Therefore, to uniformly distribute signal energy over the spectrum range of interest, binary sequence excitation methods are investigated for EIS measurements, e.g., Pseudo-Random Binary Sequence (PRBS) in [19] and Discrete-interval binary sequence (DIBS) in [20].

This paper proposes an online EIS method integrated within a three-phase neutral point clamped (NPC) converter using a multi-sine excitation. Unlike most existing studies which focus on DC/DC converters, the NPC converter operates as a DC/AC inverter. The structure of the NPC inverter allows for performing online EIS by injecting zero-sequence voltages to the inverter's references, which does not distort its output currents. Moreover, according to the proposed method, the phases of the multi-sine excitation components are optimised to maximize the battery voltage/current perturbations, while preventing inverter overmodulation. Sections II and III describe the method's operating principles and multi-sine signal optimisation, while Sections IV and V present the simulation model and results verifying the accuracy of the proposed approach.

II. NPC Converter-Based EIS

The proposed NPC converter-based EIS method is illustrated in Fig. 2. The key novelty of the structure lies in connecting the NPC's neutral point to the mid-voltage point of the battery bank and applying EIS perturbation signal via zero-sequence voltage injection into the inverter's voltage references. Injecting a zero-sequence voltage component results in charging/discharging current with distinct frequency components into/from the battery banks. Nevertheless, the zero-sequence voltage injection does not adversely affect the output power quality, since the injected zero-sequence terms are cancelled in line voltages and currents. It is noted that the above approach is not applicable to conventional two-level inverters, due to the lack of a neutral point connection at their DC-bus.

The typical interest frequency range in the electrochemical impedance spectrum for lithium batteries is from 0.01 Hz to 10 kHz [21] – [22]. Considering the sampling theorem requirement, the maximum sample frequency would be at least 20 kHz to cover a spectrum up to 10 kHz. The sampling frequency is the PWM carrier frequency ($f_{carrier}$) in the

TABLE I. Reported Power Converter-Based Broadband EIS Methods

Excitation	Converter Topology	f_{sw}	Energy Storage Type	EIS Bandwidth	Ref.
Multi-sine	Fuel cell sourced DC/DC, synchronous boost	100 kHz	PEM fuel cell	0.1 Hz to 5 kHz	[12]
Multi-sine	Battery sourced DC/DC, boost	100 kHz	Lead-acid battery	0.1 Hz to 10 Hz	[13]
Sweep Sine, Multi-sine, Chirp	Battery sourced DC/DC, buck-boost	20 kHz	Lead-acid battery, Li NMC battery	0.02 Hz to 2 kHz	[14]
Multi-sine	Battery charger DC/DC, buck	20 kHz	Li-ion battery	0.1 Hz to 5 kHz	[15]
Multi-sine	Bidirectional application DC/DC, synchronous buck	200 kHz	Li-ion battery	40 Hz to 200 Hz	[16]
Chirp	Battery charger DC/DC, phase-shifted full-bridge	60 kHz	Lead-acid battery	0.1 Hz to 1 kHz	[17]
Step	Battery sourced DC/DC, sybchronous boost	200 kHz	Li-ion battery	10 Hz to 9 kHz	[18]
PRBS	Battery charger AC/DC, Full active rectifier	85 kHz	Li NMC battery	50 Hz to 300 Hz	[19]
DIBS	Battery sourced DC/DC, synchronous boost	40 kHz	Li-ion battery	0.1 Hz to 1 kHz	[20]

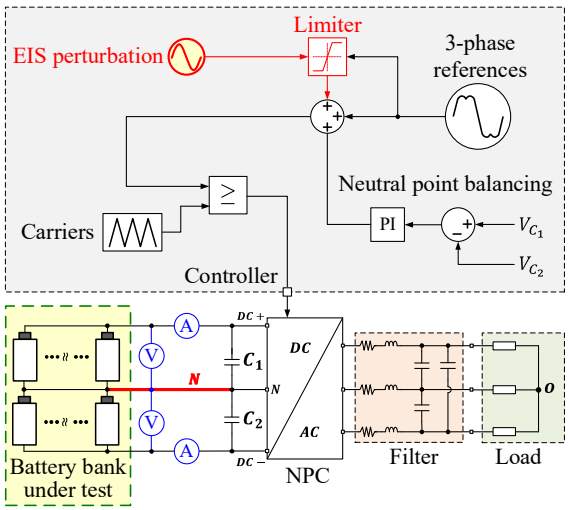

Fig. 2. Proposed three-phase NPC converter-based EIS method.

proposed method. In [23], it can be found that the battery equivalent circuit's (ECM's) resistance dominates the impedance at the high frequency of the impedance spectrum (>500 Hz), where the double layer capacitance and Warburg impedance become negligible. Hence, the battery impedance ranges from 0.01 Hz to 4 kHz still provides sufficient information for battery diagnosis and management. This allows the converter switching frequency to set to 10 kHz, which avoids excessive switching losses in the NPC inverter. To estimate impedance, a set of lock-in amplifiers are used to extract the corresponding phasor quantities of the voltages and currents and then calculate the battery impedance at different frequencies. The process is repeated over an appropriately selected frequency range, as discussed in the following section.

III. Overmodulation Prevention Optimisation

To generate high-quality output currents, inverter overmodulation must be avoided. Overmodulation can be caused by zero-sequence voltage injection, as this typically increases the peak values of the reference voltages. Thus, the inverter modulation index needs to be maintained below 1 to leave some space for zero-sequence voltage injection, while the waveform of the latter must be such that the peaks of the resulting reference voltages do not exceed 1 either. For the case of single-sine excitation, it is straightforward to select the amplitude of the injected zero-sequence voltage so that the above condition is met. With reference to multi-sine excitation, however, the frequencies, amplitudes and phases of the different sine waves must be carefully selected to avoid overmodulation. In this study, 5 frequencies were used to form each multi-sine zero-sequence voltage signal, spread evenly between two successive base frequencies, as shown in Table II. The inverter was assumed to operate with modulation index M = 90%, while the amplitudes of all sine waves were set to 10% of the DC-link voltage, V_{DC}. Depending on the phases of the sine waves, the peak values of the reference voltages could therefore reach 1.4 × V_{DC}, which would cause severe overmodulation. Overmodulation could be avoided by reducing the amplitude of the sine waves, but this would also reduce the respective battery voltage/current signals required for EIS. The measures in the following two paragraphs are therefore proposed in this paper, which guarantee that a) the inverter will not overmodulate, and b) the EIS measurements will be maximized for a given inverter modulation index and sine wave frequencies.

TABLE II. Multi-Sine Excitation Signal Frequencies and Optimised Phases

Order	1	2	4	6	8
1st base	0.01 Hz	0.02 Hz	0.04 Hz	0.06 Hz	0.08 Hz
	50°	300°	150°	0°	250°
2nd base	0.1 Hz	0.2 Hz	0.4 Hz	0.6 Hz	0.8 Hz
	75°	45°	15°	350°	310°
3rd base	1 Hz	2 Hz	4 Hz	6 Hz	8 Hz
	330°	235°	45°	165°	300°
4th base	10 Hz	20 Hz	40 Hz	60 Hz	80 Hz
	180°	160°	0°	180°	0°
5th base	100 Hz	200 Hz	400 Hz	600 Hz	800 Hz
	335°	105°	55°	235°	105°
6th base	1000 Hz	2000 Hz	4000 Hz	-	-
	0°	0°	225°	-	-

A. Limiting of the Zero-Sequence Voltage Amplitude

If V_a , V_b , V_c are the three-phase inverter references normalised to the DC-link voltage, the normalised injected multi-sine zero-sequence voltage is limited between the two values below:

$$V_{z,min} = -V_{pk} - \min\{V_a , V_b , V_c\} \quad (1)$$

$$V_{z,max} = V_{pk} - \max\{V_a , V_b , V_c\} \quad (2)$$

where V_{pk} is the desired peak value of the normalised reference waveforms. To allow for zero-sequence voltage injection, V_{pk} must be higher than the inverter modulation index, while to prevent overmodulation, it must be lower or equal to 1:

$$M < V_{pk} \leq 1 \quad (3)$$

Setting V_{pk} to 1 results in a discontinuous PWM strategy, which will have an effect on the output power quality. In this study, given that M was assumed to have a maximum value of 0.9, V_{pk} was set to 0.95.

B. Sine Wave Phases Optimisation

The limits described in the previous paragraph will alter the form of any multi-sine zero-sequence voltage waveform, as it clamps it between $V_{z,min}$ and $V_{z,max}$. The clamping reduces the amplitude of the voltage/current harmonics at the respective frequencies, thus hindering EIS measurements. Nevertheless, this effect can be minimized by appropriately setting the phases of the multi-sine waveform. Namely, for a given set of frequencies (listed in Table II) the 5 phases of the sine waves must be selected so that the integral of the clamped portions of the multi-sine waveform is minimised. Due to the large number of variables involved, this task is not straightforward to perform analytically. Thus, the proposed approach is to employ an optimisation algorithm, namely the Particle Swarm Optimisation (PSO) algorithm [24], for determining the optimal phases. The objective function of the PSO algorithm is defined as follows:

$$\underset{\boldsymbol{X}=[\varphi_1,\varphi_2,\varphi_4,\varphi_6,\varphi_8]}{\text{minimize}} f(\boldsymbol{X}) \tag{4}$$

The design variables $\varphi_1 \ldots \varphi_8$ stand for the phases of the multi-sine voltage, V_{ms}, consisting of 5 sine waves with angular frequencies $\omega_1 \ldots \omega_8$, respectively, all with amplitude A. The multi-sine voltage lost due to clamping, as a function of time, is represented by V_{lost}, while the period, T, of the integral for $f(\boldsymbol{X})$ is set according to the fundamental (output), f_o, and base frequency, f_1:

$$V_{ms} = A \times \sum_{i=1,2,4,6,8} \sin(\omega_i t + \varphi_i) \tag{5}$$

$$V_{lost} = \begin{cases} V_{ms} - V_{z,max}\,, & \text{if } V_{ms} > V_{z,max} \\ 0\,, & \text{if } V_{z,min} < V_{ms} < V_{z,max} \\ \left|V_{ms} - V_{z,min}\right|, & \text{if } V_{ms} < V_{z,min} \end{cases} \tag{6}$$

$$T = \frac{1}{\min\{f_o\,, f_1\}} \tag{7}$$

$$f(\boldsymbol{X}) = \int_0^T V_{lost}\, \mathrm{d}t \tag{8}$$

Furthermore, for given values of M and V_{pk}, the optimisation procedure can be performed offline, by generating $V_a\,, V_b\,, V_c$ numerically according to the inverter modulation strategy and calculating $V_{z,min}$ and $V_{z,max}$ from (1) – (2). This approach was adopted in this paper, assuming that the selected modulation strategy was the carrier-based equivalent of Space Vector Modulation (SVM), for which the injected zero-sequence voltage is:

TABLE III. MODEL PARAMETERS OF THREE-PHASE NPC INVERTER AND SIMPLIFIED LITHIUM-ION BATTERY ECM

Parameter		Value	Unit
V_{DC}	DC input voltage	800	V
C_{C1}, C_{C2}	DC-link capacitors	4.08	mF
L_f	Output filter inductors	0.05	mH
C_b	Delta-connected capacitors	340	μF
R_{ld}	Load resistance per phase	4	Ω
L_{ld}	Load inductance per phase	6.56	mH
f_o	Load frequency	50	Hz
$f_{carrier}$	Carrier frequency	10	kHz
OCV	Open-circuit voltage	3.7	V
R_S	Series resistor	76.4	mΩ
R_{ct}	Charge transfer resistance	47	mΩ
C_{dl}	Double-layer capacitance	1.731	F
R_{W_1}	Parallel resistance for Warburg impedance approximation	20	mΩ
C_{W_1}	Parallel capacitance for Warburg impedance approximation	5500	F
R_{W_2}	Parallel resistance for Warburg impedance approximation	30	mΩ
C_{W_2}	Parallel capacitance for Warburg impedance approximation	450	F
R_{W_3}	Parallel resistance for Warburg impedance approximation	170	mΩ
C_{W_3}	Parallel capacitance for Warburg impedance approximation	6000	F
N_{bat_s}	Number of battery cells in series	216	
N_{bat_p}	Number of battery cells in parallel	100	

$$V_{z,SVM} = \frac{\max\{V_a\,, V_b\,, V_c\} + \min\{V_a\,, V_b\,, V_c\}}{2} \tag{9}$$

The PSO algorithm was executed in MATLAB (particle swarm function) once for each Base frequency, with a swarm size of 40 particles and 20 maximum iterations. The derived phases for each sine wave, shown in Table II, were used in the simulations presented in Section V.

IV. SIMULATION MODEL

This section outlines the battery and power circuit modelling using MATLAB/Simulink to validate the proposed approach.

A. Lithium-Ion Battery Model

A simplified equivalent circuit model (ECM), Randles equivalent circuit, is taken for lithium-ion battery modelling to represent the electrochemical and physical properties of batteries for simulation, shown in Fig. 3. The open circuit voltage (OCV) is a function of the state of charge. The series resistor (R_S) represents the electrolyte and electrodes resistance. The capacitor (C_{dl}) represents the double-layer capacitance that models the charging behaviour at the electrode-electrolyte interface, and the resistor (R_{ct}) represents the charge transfer resistance for modelling the load-related voltage drop over the interface of the electrolyte and electrode. To model the lithium ions diffusion behaviour in batteries, a frequency-dependent coefficient, the Warburg impedance (Z_W) is used in Randle's ECM. However, it is not possible to model the Warburg diffusion behaviour using ordinary differential equations, Laplace transforms, or basic electric circuit elements. Therefore, this paper uses three R_wC_w branch circuits to approximate the Warburg impedance. The drawback of this approximation method is that R_wC_w need to vary with battery temperature to fit

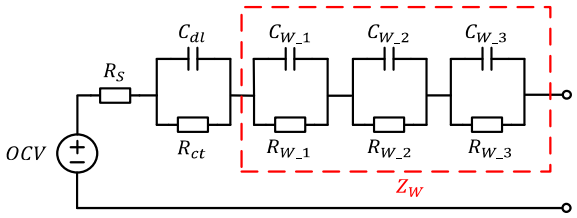

Fig. 3. Equivalent circuit model approximation of for the Warburg impedance using three R_wC_w branches.

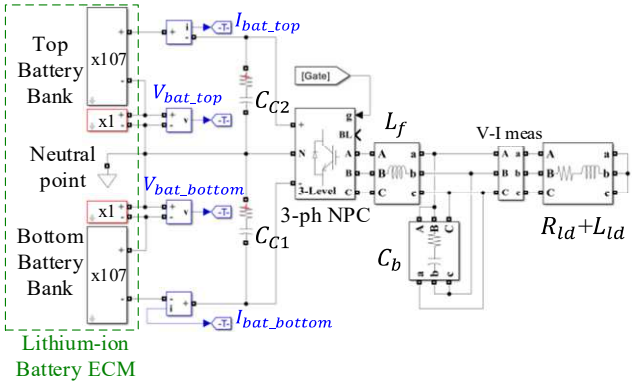

Fig. 4. Top level diagram of the proposed battery connected three-phase NPC inverter Simulink mode.

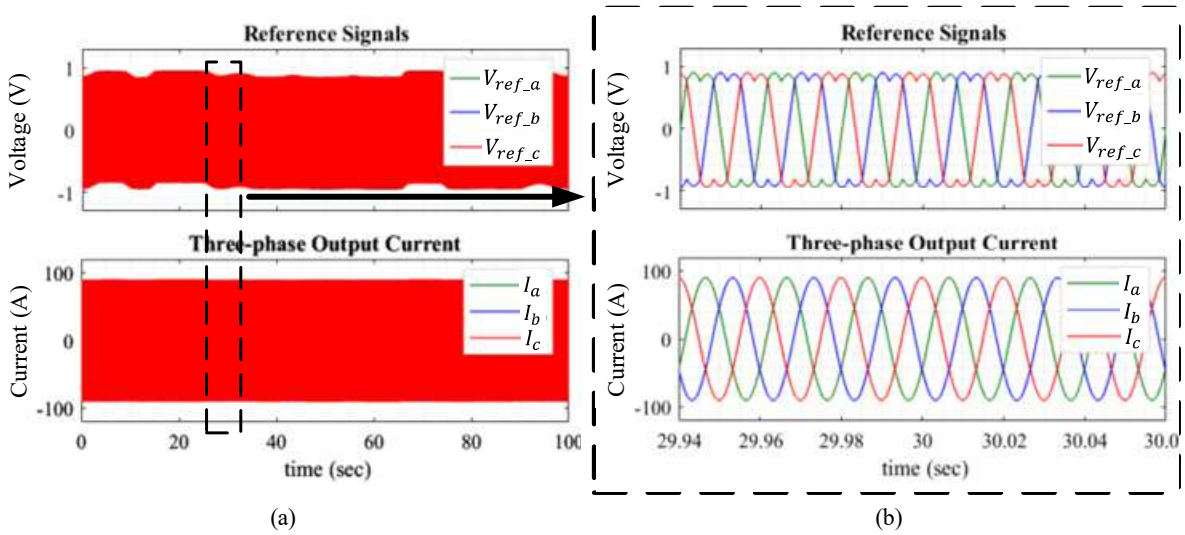

Fig. 5. Waveforms for the proposed NPC inverter-based online EIS control with 0.01 Hz perturbation: (a) normalized reference voltage (top) and output current (bottom); (b) zoomed part of the inverter waveforms in (a).

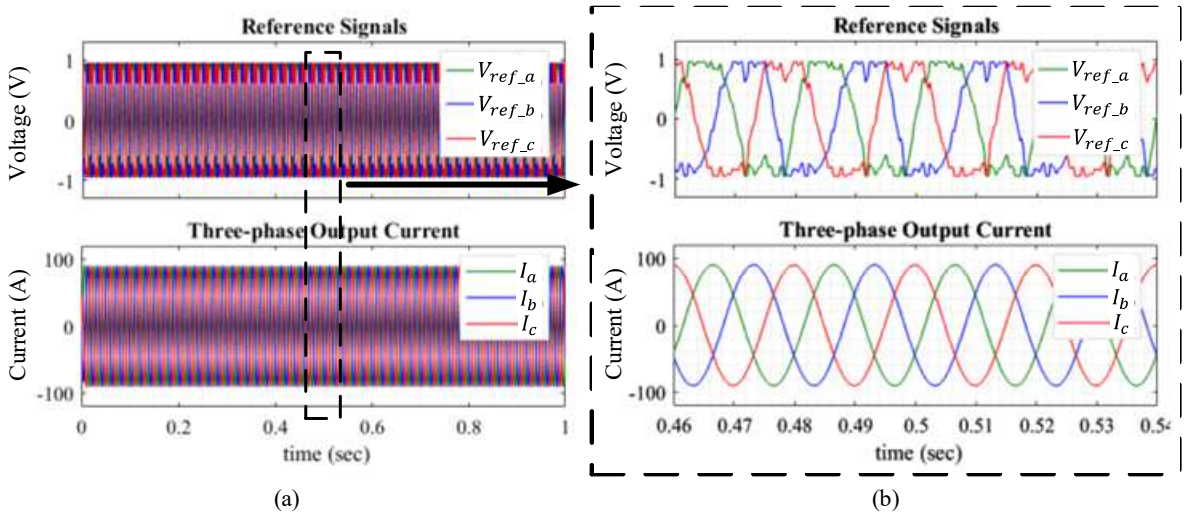

Fig. 6. Waveforms for the proposed NPC inverter-based online EIS control with 100 Hz perturbation: (a) normalized reference voltage (top) and output current (bottom); (b) zoomed part of the inverter waveforms in (a).

diffusion behaviour in reality [25]. Still, using the model to verify the EIS measurement method in simulation is reasonable. The simplified battery ECM parameters from [26] – [27] are presented in Table III. The battery bank comprises a 216 series-connected × 100 parallel-connected 3.7 V cells matrix, giving a total DC-link voltage (V_{DC}) of approximately 800 V.

B. Power Circuit Model

The battery bank is used as the input DC voltage source for the NPC converter. The neutral point of the NPC converter is connected between the top and bottom halves of the battery bank. Two DC-link capacitors, C_1 and C_2, to provide a low-impedance path for the pulsating currents at the DC side. At the inverter output, a three-phase inductor (L_f) and a set of delta-connected capacitors (C_b) are connected to filter PWM ripple. The inverter's load is a star-connected three-phase RL load with resistance R_{ld} and inductance L_{ld}. All simulation model parameter values are given in Table III.

V. Results and Discussion

The simulation results in Figs. 5 – 8 confirm that the multi-sine EIS perturbation applied via the zero-sequence voltage injection does not distort the inverter output currents, while accurately estimating the battery EIS spectrum in the frequency range of interest.

Fig. 5 refers to the case of applying the proposed method with a base frequency of 0.01 Hz. Figs. 5(a) and (b) illustrate the inverter reference voltages and output currents. It can be observed that the reference signals are clipped and limited between $\pm$ 0.95 (= V_{pk}). Nevertheless, the induced distortion on the inverter phase voltages does not affect the output current quality, which remains sinusoidal. As explained in Section II, this is because the injected component is zero-sequence (i.e., common-mode), is cancelled between the phases and thus does not affect the inverter line voltages. Figs. 6(a) and (b) illustrate the waveforms for the base frequency of 100 Hz. In both cases,

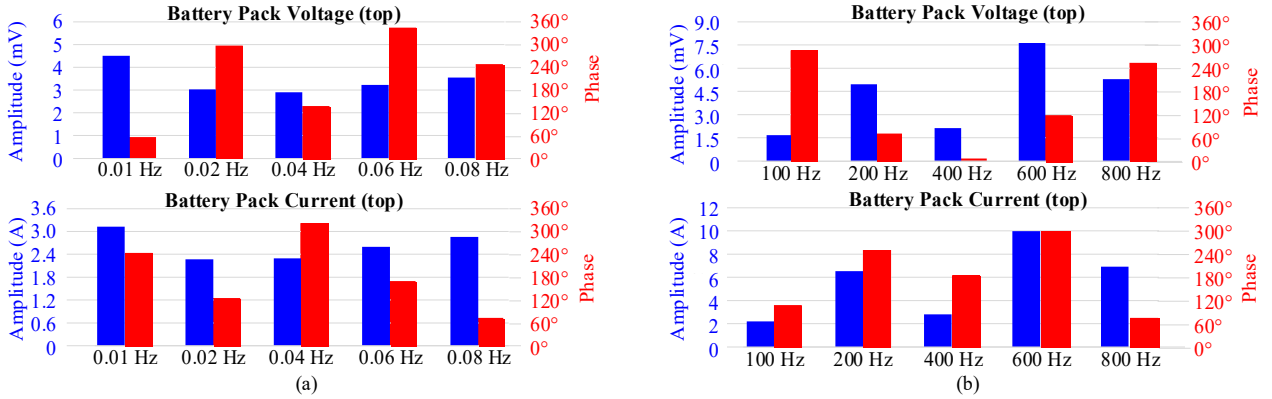

Fig. 7. The amplitude and phase of the voltage/current harmonics (for the top side battery pack) are derived from the lock-in amplifiers.

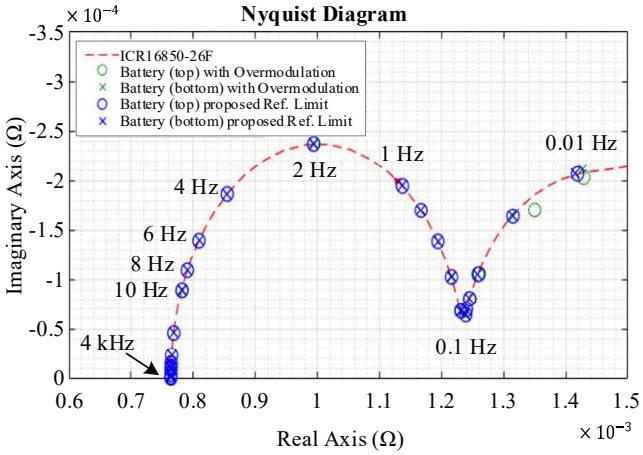

Fig. 8. Impedance Nyquist plot of the battery from 0.01 Hz to 4 kHz; comparing the theoretical impedance value to the proposed method's estimates (blue) and the estimates when operating with overmodulation (green).

multi-sine phase optimisation has been applied, reducing the part of the excitation signal loss. The bar charts in Fig. 7 present the amplitude and phase of the voltage/current harmonics (for the top battery pack) at the respective frequencies shown in Table II, derived from the lock-in amplifiers. Division of (complex) voltage by current gives the battery impedance at each frequency. It is noted that suitable voltage measuring equipment will be required in practice, since the amplitudes of the voltage harmonics are in the order of a few mV for each 3.7 V battery pack.

Fig. 8 presents the EIS impedance Nyquist diagram for the entire frequency range of 0.01 Hz to 4 kHz. The red dashed line represents the simplified ICR18650-26F ECM impedance obtained from the Laplace transform. The impedance values estimated by the proposed method are shown as blue o/x marks for the top/bottom battery pack, respectively. It can be observed that the battery pack electrochemical impedance spectrum estimated by the simulations is aligned with the theoretical values. Moreover, indicative results for the case of allowing inverter overmodulation (i.e., not applying the proposed zero-sequence voltage-limiting technique) are shown with green marks in the graph. It can be seen that overmodulation adversely affects the accuracy of the EIS measurements, as the relevant estimates deviate from the theoretical values. Besides, the inverter output currents are distorted in this case, as well. The proposed method avoids both downsides.

VI. Conclusion

In this work, an NPC inverter-based multi-sine EIS method was presented. Its novelty lies in using the unique characteristic of the NPC inverter structure to connect its neutral point and the mid-voltage point of the battery bank and then producing the perturbation on battery packs via zero-sequence voltage injection, which, unlike existing methods, does not deteriorate the quality of the inverter output voltages and currents. Furthermore, the proposed optimised multi-sine excitation prevents inverter overmodulation and offers a shorter measuring time than single-frequency excitation methods. The method has been verified using detailed simulations which confirm its accuracy over the typical EIS frequency range for lithium batteries.

References

[1] M. E. Orazem and B. Tribollet, *Electrochemical impedance spectroscopy*. Hoboken, NJ: Wiley, 2017.

[2] O. Bethoux, M. Hilairet, and T. Azib, "A new on-line state-of-health monitoring technique dedicated to PEM fuel cell," *2009 35th Annual Conference of IEEE Industrial Electronics*, 2009.

[3] W. Huang and J. A. Qahouq, "An online battery impedance measurement method using DC–DC power converter control," *IEEE Transactions on Industrial Electronics*, vol. 61, no. 11, pp. 5987–5995, 2014.

[4] D. Depernet, A. Narjiss, F. Gustin, D. Hissel, and M.-C. Péra, "Integration of electrochemical impedance spectroscopy functionality in proton exchange membrane fuel cell power converter," *International Journal of Hydrogen Energy*, vol. 41, no. 11, pp. 5378–5388, 2016.

[5] Y.-D. Lee, S.-Y. Park, and S.-B. Han, "Online embedded impedance measurement using high-power battery charger," *IEEE Transactions on Industry Applications*, vol. 51, no. 1, pp. 498–508, 2015.

[6] S. M. Islam and S.-Y. Park, "Precise online electrochemical impedance spectroscopy strategies for Li-Ion Batteries," *IEEE Transactions on Industry Applications*, vol. 56, no. 2, pp. 1661–1669, 2020.

[7] X. Wang, X. Wei, Q. Chen, and H. Dai, "A novel system for measuring alternating current impedance spectra of series-connected lithium-ion batteries with a high-power dual active bridge converter and distributed sampling units," *IEEE Transactions on Industrial Electronics*, vol. 68, no. 8, pp. 7380–7390, 2021.

[8] S. K. Dam and V. John, "High resolution converter for battery impedance spectroscopy," *2016 IEEE International Conference on Power Electronics, Drives and Energy Systems (PEDES)*, 2016.

[9] H. Wang, A. Gaillard, and D. Hissel, "Online electrochemical impedance spectroscopy detection integrated with step-up converter for fuel cell

electric vehicle," *International Journal of Hydrogen Energy*, vol. 44, no. 2, pp. 1110–1121, 2019.

[10] J. Shen, H. Homayouni, and J. Wang, "Converter-based electrochemical impedance spectroscopy for high-power fuel cell stacks with resonant controllers," *IEEE Transactions on Industrial Electronics*, vol. 68, no. 9, pp. 8819–8828, 2021.

[11] P. Hong, J. Li, L. Xu, M. Ouyang, and C. Fang, "Modeling and simulation of parallel DC/DC converters for online AC impedance estimation of PEM fuel cell stack," *International Journal of Hydrogen Energy*, vol. 41, no. 4, pp. 3004–3014, 2016.

[12] N. Katayama and S. Kogoshi, "Real-time electrochemical impedance diagnosis for fuel cells using a DC–DC converter," *IEEE Transactions on Energy Conversion*, vol. 30, no. 2, pp. 707–713, 2015.

[13] R. Ferrero, C. Wu, A. Carboni, S. Toscani, M. De Angelis, H. George-Williams, E. Patelli, and P. A. Pegoraro, "Low-cost battery monitoring by converter-based electrochemical impedance spectroscopy," *2017 IEEE International Workshop on Applied Measurements for Power Systems (AMPS)*, 2017.

[14] O. Alao and P. Barendse, "Online condition monitoring of sealed lead acid & lithium nickel-cobalt-manganese oxide batteries using broadband impedance spectroscopy," *2018 IEEE Energy Conversion Congress and Exposition (ECCE)*, 2018.

[15] E. Sadeghi, M. H. Zand, M. Hamzeh, M. Saif, and S. M. Alavi, "Controllable electrochemical impedance spectroscopy: From circuit design to control and data analysis," *IEEE Transactions on Power Electronics*, vol. 35, no. 9, pp. 9933–9942, 2020.

[16] M. Abareshi, E. Sadeghi, M. Hamzeh, M. Saif, and S. M. Alavi, "Multi-purpose controllable electrochemical impedance spectroscopy using bidirectional DC–DC converter," *Journal of Energy Storage*, vol. 55, p. 105750, 2022.

[17] V.-T. Doan, V.-B. Vu, H.-N. Vu, D.-H. Tran, and W. Choi, "Intelligent Charger with online battery diagnosis function," *2015 9th International Conference on Power Electronics and ECCE Asia (ICPE-ECCE Asia)*, 2015.

[18] J. A. Qahouq and Z. Xia, "Single-perturbation-cycle online battery impedance spectrum measurement method with closed-loop control of Power Converter," *IEEE Transactions on Industrial Electronics*, vol. 64, no. 9, pp. 7019–7029, 2017.

[19] E. Locorotondo, F. Corti, L. Pugi, L. Berzi, A. Reatti, and G. Lutzemberger, "Design of a wireless charging system for online battery spectroscopy," *Energies*, vol. 14, no. 1, p. 218, 2021.

[20] H. H. Abbasali and S. Jafarabadi Ashtiani, "Online broadband battery impedance spectroscopy using current-mode boost converter," *IEEE Transactions on Instrumentation and Measurement*, vol. 71, pp. 1–8, 2022.

[21] W. Choi, H.-C. Shin, J. M. Kim, J.-Y. Choi, and W.-S. Yoon, "Modeling and applications of electrochemical impedance spectroscopy (EIS) for lithium-ion batteries", *Journal of Electrochemical Science and Technology*, vol. 11, no. 1, pp. 1–13, 2020.

[22] U. Westerhoff, K. Kurbach, F. Lienesch, and M. Kurrat, "Analysis of lithium-ion battery models based on electrochemical impedance spectroscopy", *Energy Technology*, vol. 4, no. 12, pp. 1620–1630, 2016.

[23] J. Estaller, A. Kersten, M. Kuder, T. Thiringer, R. Eckerle, and T. Weyh, "Overview of battery impedance modeling including detailed state-of-the-art cylindrical 18650 lithium-ion battery cell comparisons," *Energies*, vol. 15, no. 10, p. 3822, 2022.

[24] J. Kennedy and R. Eberhart, "Particle swarm optimization," *Proceedings of ICNN'95 - International Conference on Neural Networks*, 1995, pp. 1942-1948, vol. 4.

[25] D. Andre, M. Meiler, K. Steiner, H. Walz, T. Soczka-Guth, and D. U. Sauer, "Characterization of high-power lithium-ion batteries by electrochemical impedance spectroscopy. II: Modelling", *Journal of Power Sources*, vol. 196, no. 12, pp. 5349–5356, 2011.

[26] Samsung SDI, "Specification of product for Lithium-ion Rechargeable Cell Model: ICR18650-26F", Oct. 2009. [Revised Nov. 2009]

[27] B. Csomós, D. Fodor, and I. Vajda, "Estimation of battery separator area, cell thickness and diffusion coefficient based on non-ideal liquid-phase diffusion modeling", *Energies*, vol. 13, no. 23, p. 6238, 2020.

BIOGRAPHIES

Kai-Ping Liu (Graduate Student Member, IEEE) received the M.Sc. degree in electrical power engineering from Newcastle University, UK, in 2020. He is currently pursuing a Ph.D. in power electronics at the University of Southampton in the UK. His research interests include power electronic converter design and electric machine control development.

Georgios I. Orfanoudakis (Member, IEEE) received his MEng in electrical engineering and computer science from the National Technical University of Athens (NTUA), Greece, in 2007, and his PhD on power electronic converters from the University of Southampton, UK, in 2013. From 2012 until 2019 he worked with the University of Southampton as a Research Associate (2012 – 2014), with the Hellenic Mediterranean University as a Teaching Fellow (2014 – 2019) and with TSL Technology Ltd, as a Power Electronics R&D Engineer. In 2020 he was appointed by the Electrical and Computer Engineering department of the Hellenic Mediterranean University, Crete, Greece, as an Assistant Professor of Power Electronics and Motor Drives. His research focuses on topologies and modulation strategies of multilevel and PV inverters, and on sensorless control of motor drives.

Suleiman M. Sharkh (Senior Member, IEEE) is Professor of Electrical Machines and Drives in the Mechatronics Research Group at the University of Southampton. He is the Deputy Director of the Southampton EPSRC Energy Storage and its Applications Centre for Doctoral Training and was past Head of the Mechatronics Research Group. He has over 20 years research experience in electric machines, power electronics and their applications in transport, renewable energy and microgrids. His inventions and research, funded by industry, EPSRC and Innovate UK, have contributed to the development of several commercial products: rim driven thrusters; direct drive tidal turbine generators; submersible motors; high speed PM machines for electric turbo compounding and gas compressors; grid connected inverters; novel electric motors with integrated clutch for hybrid marine vessel propulsion; and multi-axis actuators with adaptive resonance frequency for active vibration damping. Prof Sharkh was the winner of The Engineer Energy Innovation and Technology Award 2008 for his work on novel rim driven marine thrusters and turbine generators. He is a Senior Member of the IEEE, a member of the IET and a Chartered Engineer.

Andrew Cruden received the B.Eng., M.Sc., and Ph.D. degrees in electronic and electrical engineering from the University of Strathclyde, Glasgow, UK, in 1989, 1990, and 1998, respectively. He is currently the Associate Dean (Infrastructure) of the Faculty of Engineering and Physical Sciences (FEPS) and a Professor of energy technology with the University of Southampton, U.K. He has significant experience in the field of energy storage and electric vehicles, covering vehicle-to-grid (V2G), new battery technologies, such as aluminium-ion cells, and flow cells, such as soluble lead flow battery. He has previously worked in fuel cell technology and condition monitoring of wind turbines. He is a member of the Training and Diversity Panel of the U.K.'s Faraday Institution and the Co-Director of the EPSRC Centre for Doctoral Training (CDT) in energy storage and its applications.